ORIGINAL RESEARCH   **Open Access**

A novel low voltage ride through strategy for cascaded power electronic transformer

Jiexiang Han[1*], Xiangping Kong[2], Peng Li[2], Zhe Zhang[1] and Xianggen Yin[1*]

Abstract

In view of the operating characteristics for voltage sags of AC side of the power electronic transformer(PET), a low-voltage ride through(LVRT) strategy adapted to bidirectional power exchange of PET is proposed for the purposes of maintaining the system stability, assisting the system voltage recovery and protecting PET safety. During the asymmetric voltage sag, the negative sequence current of PET is eliminated to ensure the symmetry of the injected current. According to the degree of positive sequence voltage sag, the reactive current injection is provided to assist in voltage recovery. According to the PET active power condition before the voltage sag, the level and direction of which are maintained as far as possible without exceeding the limit, for which the disturbance to the AC and DC grids is reduced. Finally, the effectiveness of the proposed LVRT strategy is verified by simulation model.

Keywords: Power electronic transformer, Low-voltage ride through, Control strategy, Current instruction value

1 Introduction

With the increase of grid-connected capacity of distributed energy and the growth of the demand for 'plug and play' of user-side load, DC power distribution technology has been gradually applied for pilot applications due to its outstanding power supply capability, strong controllability and good load compatibility [1, 2]. And traditional AC distribution network is developing towards AC/DC hybrid distribution network. As a key equipment in AC/DC hybrid distribution network, power electronic transformer(PET) bears many tasks such as AC/DC system interconnection, voltage level conversion, power flow control, power quality adjustment, reactive power compensation and so on [3–5], the operating performance of which has a vital impact on the safe and stable operation of the power grid.

In the AC/DC hybrid distribution network, the main power supply is generally an AC power supply. When the AC grid is short-circuited and the voltage sags, the PET should realize LVRT without off-grid to improve the stability of the grid operation and the reliability of the power supply. At present, there are a lot of

researches on the normal operation control strategy of PET [6–9]. However, there are relatively few studies on LVRT strategies. In [10], aiming at the asymmetric short-circuit fault on AC side, the negative sequence voltage injection method is proposed to realize the DC voltage equalization between the bridge arms, but this measure will inject negative sequence current into the grid, which will adversely affect the operation of electrical equipment. In [11], the zero sequence voltage injection method is used for DC voltage equalization control, and the negative sequence current suppression is used to reduce the negative sequence current. However, the double-loop control is still used during the LVRT, which slows down the system adjustment speed and affect the negative sequence current suppression effect. Reference [12] proposed a LVRT strategy for a cascaded H-bridge centralized photovoltaic grid-connected device, which injected reactive power into the grid during voltage sags, but the PV grid-connected device is a power unidirectional transmission device, for which this strategy does not accommodate power bidirectional transmission conditions.

According to the structural characteristics of PET, a LVRT strategy suitable for bidirectional power exchange of PET is proposed for the purpose of maintaining system stability, assisting system voltage recovery and

* Correspondence: hanjiexiang@hust.edu.cn
[1]State Key Laboratory of Advanced Electromagnetic Engineering and
Technology, Huazhong University of Science and Technology, Wuhan
430074, Hubei, China
Full list of author information is available at the end of the article

ensuring PET operation safety, which can realize reactive power support and negative sequence current elimination in short-circuit fault of power grid, and effectively reduce active power fluctuations. The good performance of the proposed LVRT strategy is verified by the simulation results.

2 Methods
2.1 Topology of PET
PET can be divided into AC/AC type and AC/DC/AC type according to whether the intermediate conversion module has DC link. The latter has become the research focus because of its good controllability and high flexibility. AC/DC/AC type PET includes two basic structural forms: cascaded H-bridge type and Modular Multilevel Converter(MMC) type [5, 13]. Cascaded H-bridge PET has advantages of higher power density, and there is no bridge arm circulating current when three-phase star connection is connected, for which its research and application have received extensive attention. This paper will focus on the engineering practice and the LVRT strategy of cascaded H-bridge PET.

The basic structure of the cascaded H-bridge four-port PET is shown in Fig. 1. The ports are AC 10 kV, DC ± 750 V, AC 380 V and DC ±375 V respectively.

The AC-DC module in Fig. 1 implements the power conversion between AC10kV and DC ± 750 V, which is a key component and bear the main function of the PET. The AC-DC module shown in Fig. 2(a) consists of two identical star cascaded units shown in Fig. 2(b). Two AC-DC converters of the same structure can realize DC bipolar output by symmetrical connection. Because the positive and negative poles of the bipolar AC-DC converter have the same topological structure, in this paper, the single-pole structure converter shown in Fig. 2(b) is studied, and the control strategy of the other pole is identical.

One of the main problems that need to be solved in the practical application of cascaded H-bridge PET is how to achieve the equalization of the three-phase DC

voltage when asymmetric voltage sags occur in the power grid to ensure the safe operation of the converter. References [11, 12] proposes the use of zero sequence or negative sequence voltage injection strategies to achieve DC voltage equalization control, but it will lead to control complexity, and the time-delay effect of the control strategy will affect the equalization effect. In view of the above problems, this paper realizes the self-balancing of DC voltage between bridge arms through the optimization design of DC link topology, which is shown in Fig. 2(b) and Fig. 3. In Fig. 2(b), the sub-module of the cascaded bridge arm adopts a typical cascaded H-bridge structure on the AC side, and on the DC side all the three-phase sub-modules are uniformly connected in parallel to form a DC port; In Fig. 3, the sub-module of AC-DC module uses a resonant bidirectional DC-DC converter, and the double-sided H-bridge is connected through a high-frequency transformer with a resonant capacitor to achieve voltage level conversion and electrical isolation. The H-bridge on both sides modulate the DC voltage into a high-frequency square wave, and the power exchange is realized through the resonance link. When the operating frequency is near the resonant frequency, the DC-DC ratio of the converter is equal to the high-frequency transformer ratio, and the performance of the converter is stable, and the load capacity of the converter is strong [14, 15].

As shown in Fig. 2(b) and Fig. 3, the DC side adopts a unified parallel port, combined with the superior performance DC-DC converter, can realize the self-balancing of the sub-module voltage; the AC side adopts the series structure, which can ensure the input current of the sub-module is consistent, so the PET can realize the sub-module voltage and current self-balancing to achieve balanced distribution of power between sub-modules. The relationship between the AC side current, the DC side voltage and the submodule voltage and current can be obtained as shown in (1).

$$\begin{cases} u_{dc_1k1} = u_{dc_1k2} = \cdots = u_{dc_1kN} = U_{dc}/n_T \\ i_{ink1} = i_{ink2} = \cdots = i_{inkN} = i_k \end{cases} \quad (1)$$

Where $k = a$, b, or c is the phase of AC side, u_{dc_1} is DC-DC converter primary side voltage, U_{dc} is DC port voltage, n_T is the high frequency transformer ratio, i_k is ac side current and i_{in} is input current of submodule.

Therefore, adopting the above topology structure, when an asymmetric voltage sag occurs on the AC side, the DC side parallel modules can realize current self-balancing, thereby realizing the AC side series modules voltage self-balancing. Thus, there is no need to add the DC voltage balance control link, for which the device operating performance can be improved and the control system can be simplified.
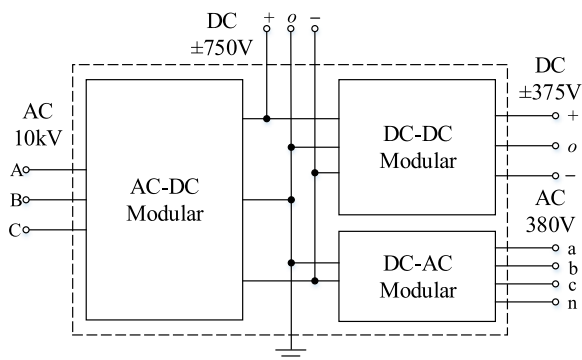

Fig. 1 PET overall structure
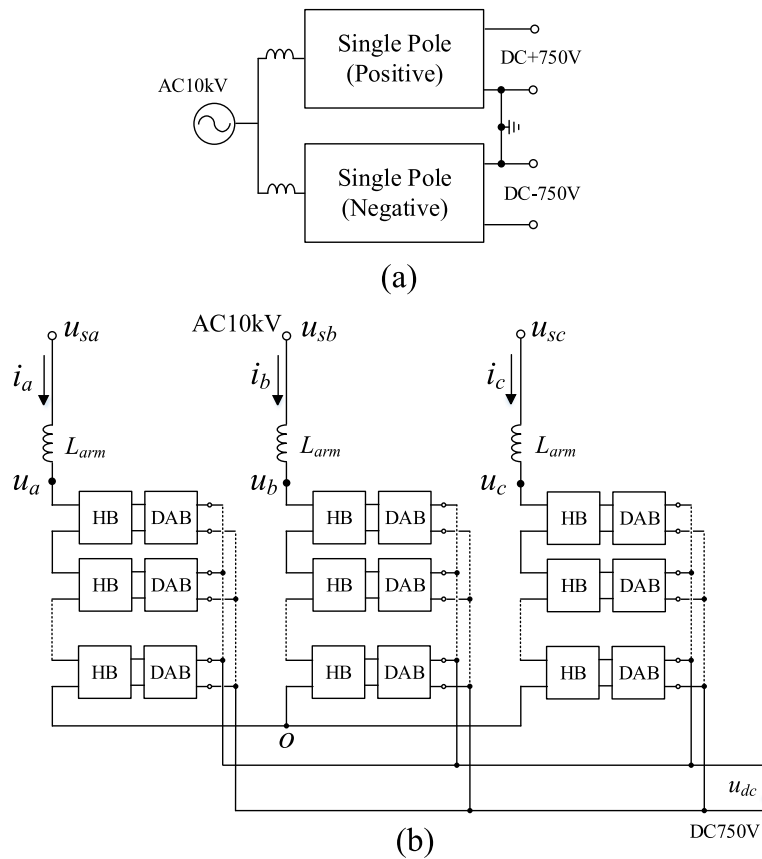
Fig. 2 PET pre-stage AC-DC module topology. **a** Bipolar AC-DC module. **b** Single-pole structure

2.2 LVRT strategy of PET

2.2.1 Control objectives of LVRT

AC-DC module of PET generally uses a dual closed-loop control strategy during normal operation, as shown in Fig. 4. According to the working conditions and control objectives of PET, the outer loop can be controlled by constant DC voltage or constant power respectively, the adjustment time of which is generally 40~100 ms. The current inner loop adopts the d-axis voltage-oriented feedforward decoupling control strategy to quickly track the d-axis and q-axis current instruction values generated by the outer loop controller to improve the control performance, and the tracking time is 2~5 ms.

In the case of AC power grid failure causing AC bus voltage drop, PET operating in constant voltage mode can transfer voltage control function to other equipment, thus the DC voltage can be maintained during the low voltage ride through operation, then blocking voltage and reactive power outer loop. When the DC bus voltage is controlled by other equipment such as energy storage systems, PET can work in constant power control mode and can directly block the outer power loop. Thus, the current inner loop is directly used for control during the LVRT operation to improve the overall response speed by blocking the outer loop of the controller.
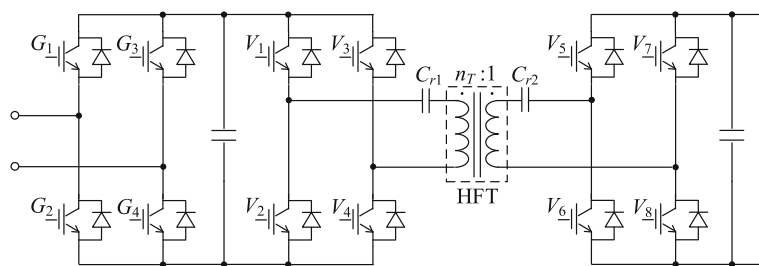
Fig. 3 PET cascaded unit sub-module topology
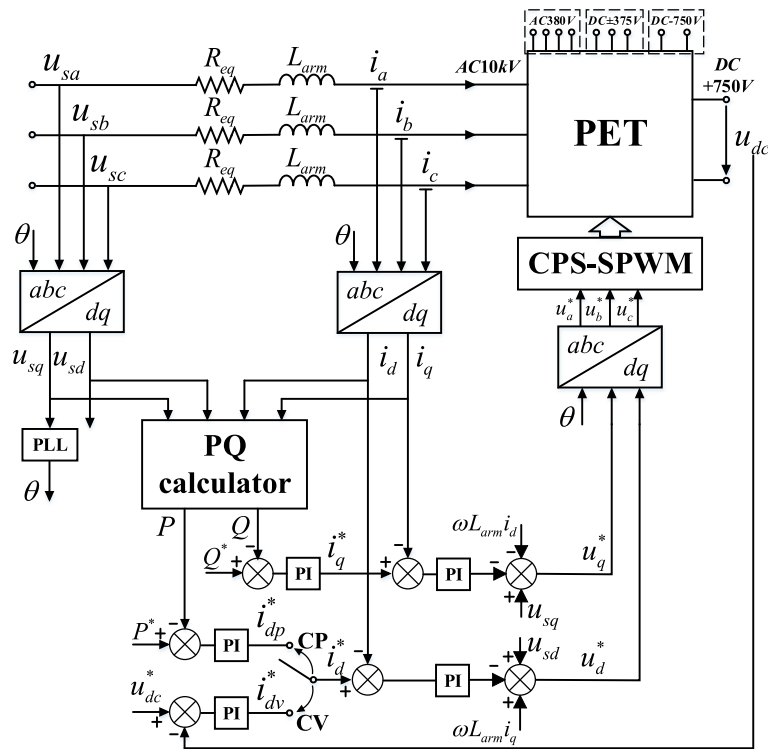
**Fig. 4** Steady state control schematic diagram of PET

When the AC grid is short-circuited and the voltage sags, the PET should realize LVRT without off-grid to improve the stability of the grid operation and the reliability of the power supply. At present, there are few researches on PET LVRT control strategies, and this paper attempts to make up for this deficiency. PET is interconnected with the AC grid via an inverter, which is similar to photovoltaic power and direct drive wind turbine. Therefore, their LVRT control targets also have similarities for the purposes of ensuring the safe operation of the inverter and maintaining the stability of grid. In the design of the LVRT strategy of this paper, the relatively mature LVRT methods of renewable energies are used for reference. The main difference between PET LVRT control and renewable energies is that the power transmission direction of the later is one-way, while PET acts as a substation device with active power, for which the power bidirectional transmission characteristics need to be considered and special treatment is required in the given algorithm of the active current instruction value in PET LVRT strategy. Moreover, as an interconnected equipment for AC-DC hybrid distribution network, PET needs to meet the requirements of power supply reliability and power quality maintenance. In this paper, for the purposes of maintaining stable operation of the power grid, assisting grid voltage recovery and ensuring the safety of PET itself, the basic control objectives of PET LVRT are proposed as follows:

1) When an asymmetric short circuit fault occurs in the power grid, the negative sequence current is eliminated by the negative sequence current suppression measures to ensure the symmetry of the current injected into the grid;

2) According to the degree of positive sequence voltage sag on the AC side, the reactive current injection is automatically adjusted to help the grid voltage recovery;

3) According to the active power condition before the voltage sag and the degree of positive sequence voltage sag on the AC side, the active transmission level and direction are maintained as far as possible under the premise of ensuring that the PET current does not exceed the limit, for which the disturbance to the AC/DC grid is reduced.

The block diagram of the LVRT strategy is shown in Fig. 5, In which α is the positive sequence voltage sag degree, which is the ratio of the positive sequence voltage amplitude during voltage sag to the normal operation voltage amplitude, that is:

$$\alpha = u_{sd+}^{+}/u_{sd0} \tag{2}$$

When PET detects $\alpha < 0.9$, it is switched to LVRT control mode automatically. In the case of AC power grid
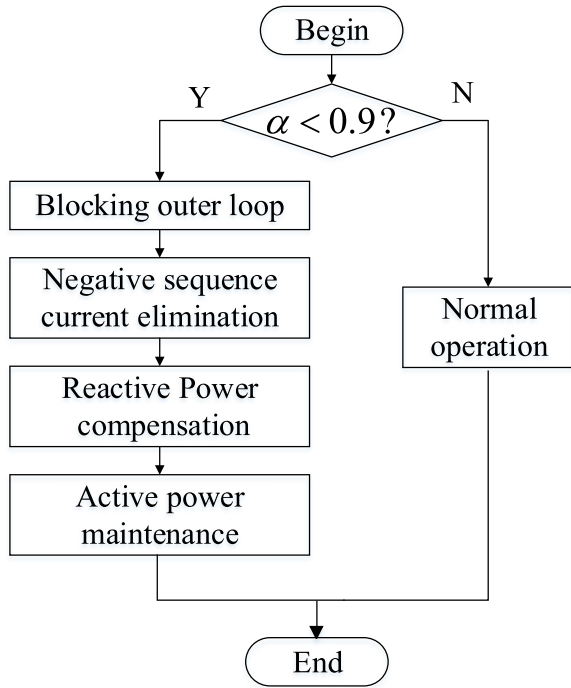
Fig. 5 LVRT strategy of PET

failure causing AC bus voltage drop, it is considered that the energy storage equipment is connected to the DC grid, for which the DC voltage can be maintained during the low voltage ride through operation. The current inner loop is directly used for control to improve the overall response speed by blocking the outer loop of the controller.

2.2.2 Implementation of LVRT

A. Inner loop design

The PET pre-stage AC-DC converter realizes the power conversion between AC and bipolar DC. The transformation modules of the two star cascaded structures are identical, so the mathematical model and control strategy are also identical. Therefore, this section only discusses the transformation module between the AC side and the unipolar DC.

The mathematical model of the AC side of the AC-DC module of PET shown in Fig. 2 is

$$
\begin{cases}
L_{arm}\dfrac{di_a}{dt} + R_{eq}i_a = u_{sa} - u_a \\
L_{arm}\dfrac{di_b}{dt} + R_{eq}i_b = u_{sb} - u_b \\
L_{arm}\dfrac{di_c}{dt} + R_{eq}i_c = u_{sc} - u_c
\end{cases}
\tag{3}
$$

In (3), L_{arm} is the bridge arm filter inductor, R_{eq} is the series equivalent resistance of the IGBT turn-on resistors

of cascaded H-bridge sub-module and filter inductor additional resistor, u_{sa}, u_{sb} and u_{sc} are the point of common connection (PCC) voltage, i_{sa}, i_{sb} and i_{sc} are the grid-connected current, u_a, u_b and u_c are multi-level voltages obtained by superimposing the output of sub-module on the AC side of the AC-DC module.

The overall mathematical model of the AC-DC module in the three-phase stationary coordinate system shown in (3) is not conducive to the control system design, and it can be transformed into a two-phase rotating coordinate system, that is

$$
\begin{cases}
L_{arm}\dfrac{di_d}{dt} + R_{eq}i_d = u_{sd} - u_d + \omega L_{arm}i_q \\
L_{arm}\dfrac{di_q}{dt} + R_{eq}i_q = u_{sq} - u_q - \omega L_{arm}i_d
\end{cases}
\tag{4}
$$

During voltage asymmetric sags, the system voltage and current will contain positive and negative sequence components. Performing positive and negative sequence decomposition on mathematical model shown in (4) in a double dq coordinate system, and the AC side mathematical model of the AC-DC module of PET in the forward and the reverse rotation coordinate system can be obtained as (5) and (6).

$$
\begin{cases}
L_{arm}\dfrac{di_{d+}^+}{dt} + R_{eq}i_{d+}^+ = u_{sd+}^+ - u_{d+}^+ + \omega L_{arm}i_{q+}^+ \\
L_{arm}\dfrac{di_{q+}^+}{dt} + R_{eq}i_{q+}^+ = u_{sq+}^+ - u_{q+}^+ - \omega L_{arm}i_{d+}^+
\end{cases}
\tag{5}
$$

$$
\begin{cases}
L_{arm}\dfrac{di_{d-}^-}{dt} + R_{eq}i_{d-}^- = u_{sd-}^- - u_{d-}^- - \omega L_{arm}i_{q-}^- \\
L_{arm}\dfrac{di_{q-}^-}{dt} + R_{eq}i_{q-}^- = u_{sq-}^- - u_{q-}^- + \omega L_{arm}i_{d-}^-
\end{cases}
\tag{6}
$$

The '+' in the lower corner of each variable in the equation represents the forward rotation coordinate system, and the '-' represents the reverse rotation coordinate system. The '+' in the upper corner indicates the positive sequence component, and the '-' indicates the negative sequence component.

The PI controller is used for current regulation and current feedforward decoupling. According to the mathematical models shown in (5) and (6), the positive and negative sequence dq axis voltage instruction values can be obtained as (7) and (8), the corresponding LVRT block diagram is shown in Fig. 6.

$$
\begin{cases}
u_{d+}^{+*} = -\left[k_p\left(i_{d+}^{+*} - i_{d+}^+\right) + k_i\int\left(i_{d+}^{+*} - i_{d+}^+\right)dt\right] \\
\qquad + u_{sd+}^+ + \omega L_{arm}i_{q+}^+ \\
u_{q+}^{+*} = -\left[k_p\left(i_{q+}^{+*} - i_{q+}^+\right) + k_i\int\left(i_{q+}^{+*} - i_{q+}^+\right)dt\right] \\
\qquad + u_{sq+}^+ - \omega L_{arm}i_{d+}^+
\end{cases}
\tag{7}
$$
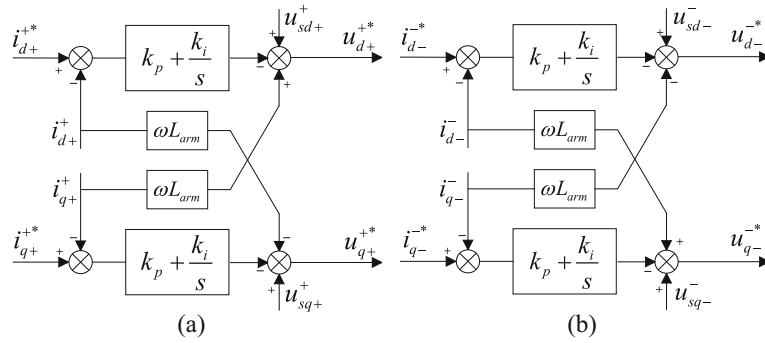
Fig. 6 Voltage asymmetric sag current inner loop control block diagram (**a**) Positive sequence components in forward rotation coordinate system (**b**) Negative sequence component in reverse rotation coordinate system

$$\begin{cases} u_{d-}^{-*} = -\left[k_p \left(i_{d-}^{-*} - i_{d-}^{-} \right) + k_i \int \left(i_{d-}^{-*} - i_{d-}^{-} \right) dt \right] \\ \qquad + u_{sd-}^{-} - \omega L_{arm} i_{q-}^{-} \\ u_{q-}^{-*} = -\left[k_p \left(i_{q-}^{-*} - i_{q-}^{-} \right) + k_i \int \left(i_{q-}^{-*} - i_{q-}^{-} \right) dt \right] \\ \qquad + u_{sq-}^{-} + \omega L_{arm} i_{d-}^{-} \end{cases} \quad (8)$$

The unified control block diagram model after decoupling the current inner loop is shown in Fig. 7, in which x^* and x represent the current instruction values and actual values in Fig. 6(a) and Fig. 6(b) respectively. The design principle of the current inner loop PI controller in Fig. 7 is the same with that of the steady-state control strategy because the control block diagram is consistent. The current inner loop can be guaranteed to have good tracking performance by optimizing the regulator parameters. The current inner loop controller parameters are set in the light of the typical I-type system, for which the current inner loop can be equivalent to the first-order inertia unit [16], and its time constant is 2~5 ms.

B. Negative sequence current elimination

During the asymmetric voltage sag of the grid voltage, Negative sequence current is eliminated in order to ensure the symmetry of the three-phase current injected into the grid to reduce the impact on the grid, as shown in (9). The negative sequence current dq-axis component instruction value in the reverse rotation coordinate

system shown in Fig. 6(b) is given as zero, and the negative sequence current dq-axis component will quickly follow the instruction value shown in (9) to achieve the function of negative sequence current elimination.

$$\begin{cases} i_{d-}^{-*} = 0 \\ i_{q-}^{-*} = 0 \end{cases} \quad (9)$$

C. Reactive power injection

The q-axis positive sequence current instruction value is shown in (10). In the case of a voltage sag of less than 10%, PET can operate stably according to the normal control strategy, at this time $i_{q+}^{+*} = 0$ to achieve unit power factor operation. When the voltage sags by more than 10%, for every 10% sag, PET provides 15% reactive power compensation to the AC grid, supporting the PCC voltage of the grid to help restore the grid voltage. The maximum compensation capacity of PET is 1.2 times the rated current.
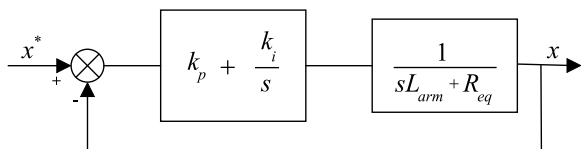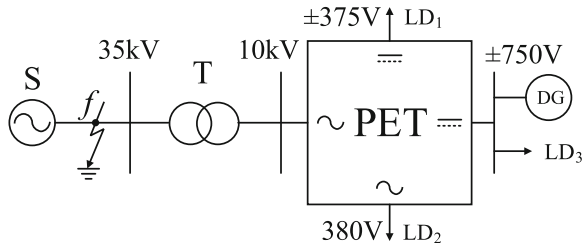

Fig. 7 Current inner loop unified control block diagram
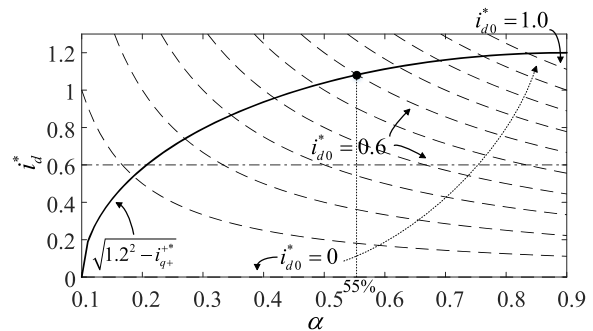
Fig. 8 Schematic diagram of active current compensation capability

Fig. 9 simulation system model of PET

$$i_{q+}^{+*} = \begin{cases} 0 & , \alpha > 0.9 \\ 1.5(0.9-\alpha) & , 0.1 < \alpha < 0.9 \\ 1.2 & , \alpha < 0.1 \end{cases} \quad (10)$$

D. Active power maintenance

The main practice of renewable energies to achieve LVRT is to perform dynamic reactive power support according to the degree of system voltage drop, but the instruction value of active current is not clearly defined. Based on the dynamic reactive power support, the LVRT strategy proposed in this paper gives a novel active current instruction value algorithm to maintain the transmission direction and level of active power of PET in normal and LVRT conditions as much as possible, thus reducing the disturbance to the AC-DC hybrid distribution network.

During the grid voltage sag, the active power absorbed by PET from the grid is shown in (11).

$$p = u_{sd+}^{+}i_{d+}^{+} + u_{sq+}^{+}i_{q+}^{+} + u_{sd-}^{-}i_{d-}^{-} + u_{sq-}^{-}i_{q-}^{-} \quad (11)$$

When the positive sequence d-axis voltage orientation is adopted, $u_{sq+}^{+} = 0$. During LVRT operation, the nega-

Table 1 Parameters of simulation system

Simulation parameters(unit)	value
PET rated capacity(MVA)	3
PET rated AC voltage(kV)	10
PET rated DC voltage(kV)	±0.75
PET filter inductor (H)	0.02
PET equivalent resistance (Ω)	0.01
Transformer ratio	35/10.5
Transformer capacity (MVA)	30
Leakage resistance (p.u.)	0.1
DG rated capacity(MVA)	5
±375 V DC load LD₁(MVA)	0.3
380 V AC load LD₁(MVA)	0.2
±750 V DC load LD₁(MVA)	2.5

Table 2 Low voltage ride through variables of voltage symmetric sag

	Variable	Rectified state	Inverter state
Before voltage sag	$P^*(i_{d0}^*)$	0.375	− 0.375
	$Q^*(i_{q0}^*)$	0	0
	P_0	0.375	− 0.375
	Q_0	0	0
After voltage sag $a = 0.4$	i_d^*	0.937	− 0.937
	i_q^*	0.75	0.75
	P	0.375	− 0.375
	Q	−0.3	− 0.3

tive sequence current can quickly track the instruction value of (9), that is, $i_{d-}^{-} = i_{q-}^{-} = 0$. The positive sequence d-axis current is also able to quickly track its instruction value. From the above analysis, the PET absorption power during the voltage sag can be obtained as shown in (12).

$$p = u_{sd+}^{+}i_{sd+}^{+*} \quad (12)$$

The power absorbed by PET from the grid before the grid voltage sags is

$$p_0 = u_{sd0}i_{d0}^* \quad (13)$$

PET transmission loss is neglected. It can be seen from the combination of (2), (12) and (13) that during the voltage sag, in order to maintain the active transmission level, the amplitude algorithm of the active current instruction value must be (14), which will change according to the degree of voltage drop to maintain the level of active power before and after the fault.

$$i_{d+}^{+*} = i_{d0}^*/\alpha \quad (14)$$

Therefore, the d-axis positive sequence current instruction value represented by (15) can be obtained. The level of active power exchange before the voltage sag is maintained as far as possible based on the q-axis positive
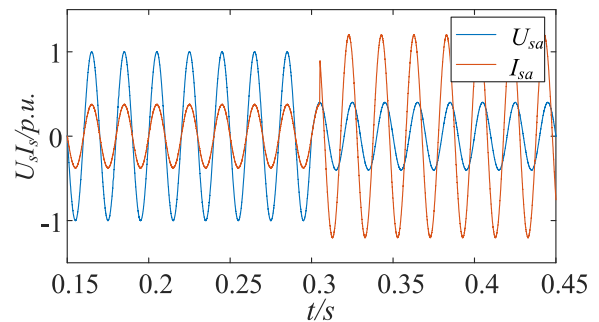
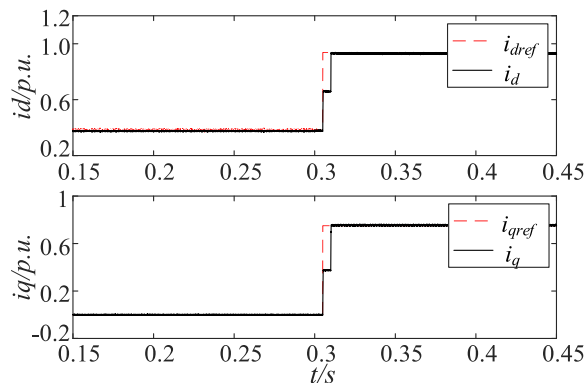**Fig. 10** Phase A voltage and current when the voltage drops in the rectified state
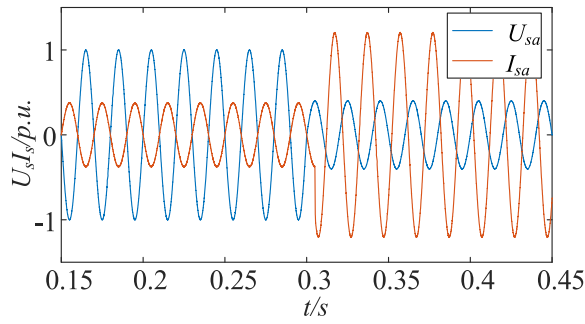
Fig. 11 Phase A voltage and current when the voltage drops in the inverter state
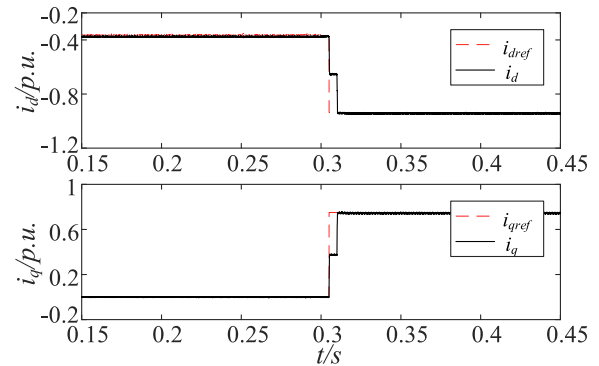
sequence current instruction value which has been given in (10), and the 1.2 times current-carrying restriction condition is considered. In (15), *sign* is a symbol function, for which the transmission direction of the active power before the voltage sag can be obtained, so that the LVRT strategy can adapt to the characteristics of the PET bidirectional power transmission. This is the adaptation and improvement of the renewable energy LVRT. $\sqrt{1.2^2 - i_{q+}^{+*2}}$ is the maximum allowable active current instruction value after reactive compensation according to (10).

$$i_{d+}^{+*} = sign(i_{d0}^*) \times \min\left\{ \left| i_{d0}^* \right| / \alpha, \sqrt{1.2^2 - i_{q+}^{+*2}} \right\} \quad (15)$$

Substituting (10) into (15), the relationship between the positive sequence active current instruction value upper limit and the positive sequence active current instruction demand value for maintaining the active level before voltage sag and the voltage sag depth is shown in Fig. 8. The solid line in the figure is the maximum allowable active current after reactive power compensation, that is, the upper limit of active current. As the voltage sag depth deepens, the reactive power demand gradually


Fig. 13 *dq*-axis current when the voltage drops in the inverter state

increases, and the active power upper limit gradually decreases. The dotted clusters in the figure represent the amount of active output required to maintain the active level before and after the voltage sag. The dotted line from bottom to top respectively indicates that the PET is from no load to full load before the voltage sag, and the interval is 0.1p.u. It can be seen from Fig. 8 that the requirement of maintaining the active level before the voltage sag can be achieved according to the (14). Taking the active current instruction value of 0.6 before the voltage sag as an example, as shown in Fig. 8, the horizontal dotted line in the figure is the active current before the voltage sag. Under the condition that the voltage sag is not less than 55%, the control strategy can ensure the active before and after the voltage sag. The transmission level and direction remain constant.
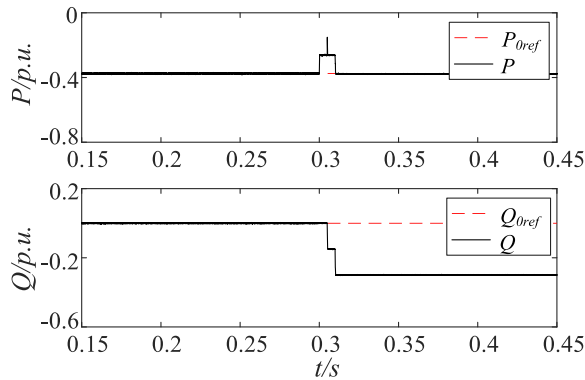
3 Simulation results and discussion

In order to verify the effectiveness of the PET LVRT strategy proposed in this paper, a four-port PET simulation model was built in PSCAD/EMTDC for simulation verification. The simulation model is shown in Fig. 9. In the simulation model, the DC bus voltage is mainly

Fig. 12 *dq*-axis current when the voltage drops in the rectified state
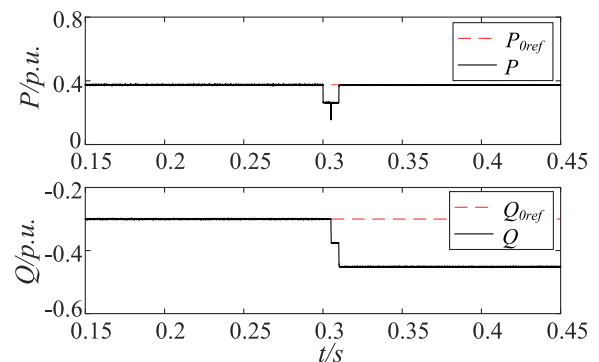
Fig. 14 Power waveform when the voltage drops in the rectified state

Fig. 15 Power waveform when the voltage drops in the inverter state

Fig. 16 Positive sequence dq-axis current when the voltage drops under no-load condition

controlled by the energy storage system with the capacity of 5 MW.

The PET is connected to the AC grid through a line-frequency transformer, and the DC side is incorporated with a ± 750 V DC bus with distributed power and DC loads. The low voltage DC port and the low voltage AC port respectively supply power to the DC and AC loads. When the symmetric short circuit and the asymmetric short circuit occur at point f, the voltage symmetry and asymmetry sag at the 10 kV bus are adjusted by adjusting the fault resistance to verify the PET LVRT strategy proposed in this paper. The main simulation parameters are shown in Table 1.

3.1 Voltage symmetric sag
Symmetric sag of three-phase voltage occurs at the connection bus of PET, the sag moment is t = 0.3 s, the degree of sag is $\alpha = 0.4$. The PET is set to operate in unit power factor of $P^* = 0.375$ and $P^* = -0.375$ before the voltage sag. The current instruction values obtained according to (9), (10) and (15) and power values measured in the simulation model are shown in Table 2.

Figures 10, 11, 12, 13, 14 and 15 are current and power simulation waveforms of the two operating

conditions shown in Table 2 in the case of voltage symmetric sag.

Figure 10 and Fig. 11 are voltage and current waveforms of phase A when the voltage drops in the rectified and inverter state.

Figures 12 and 13 show the dq-axis current instruction value and actual value waveforms. It is considered that there is 5 ms adjustment delay of the phase-locked loop(PLL), the outer loop of the controller is blocked within 5 ms after detecting that the positive sequence voltage sags, and the dq current reference value before the voltage sag is used as the inner loop instruction value. This method can prevent the power fluctuation caused by the adjustment of PLL, as well as the influence of the control system and PET for the output jitter of PLL caused by the voltage flicker on the normal operation.

Figures 14 and 15 show the waveforms of PET absorption power. After the voltage sags, PET can inject reactive power into the AC system according to the voltage sag depth to help the AC system voltage recovery. And can maintain the active transmission level before the fault.

Table 3 Low voltage ride through parameters of voltage asymmetric sag

| | Variable | No load | Full load | |
			Rectified state	Inverter state
Before Voltage sag	P^* (i_{d0}^*)	0	1	−1
	Q^* (i_{q0}^*)	0	0	0
After Voltage Sag $a = 0.4$	i_{d+}^{+*}	0	1.112	−1.112
	i_{q+}^{+*}	0.45	0.45	0.45
	i_{d-}^{-*}	0	0	0
	i_{q-}^{-*}	0	0	0
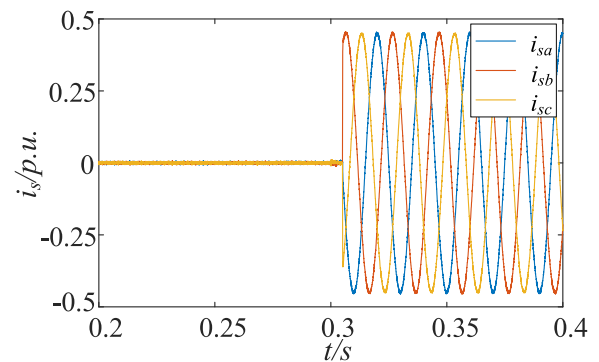
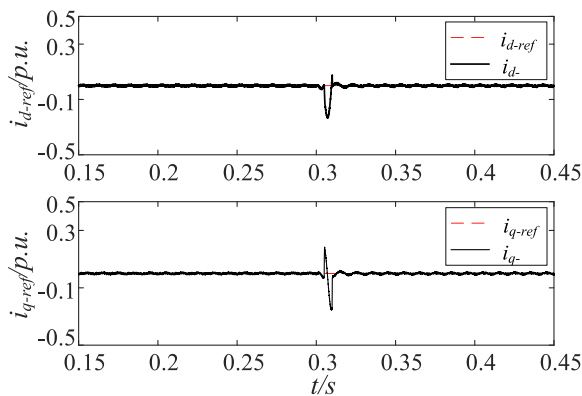**Fig. 17** Three-phase grid-connected current when the voltage drops under no-load condition
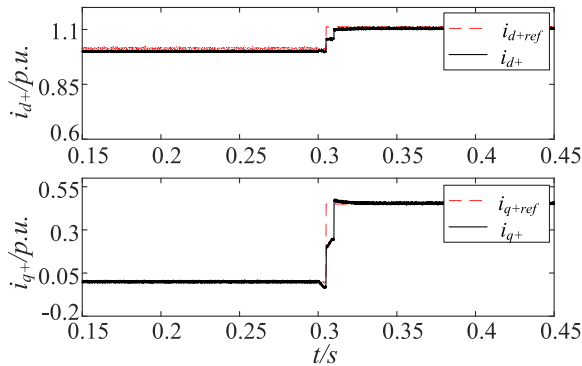
Fig. 18 Positive sequence *dq*-axis current when the voltage drops under full load condition

3.2 Voltage asymmetric sag

The A-phase voltage at the connection bus of PET is unchanged, and the amplitude of BC two-phase voltage sags to 40% of the original value. According to the symmetrical components method, the positive sequence voltage sag depth can be obtained as $\alpha = 0.6$. Under this condition, the simulation is verified for the case of no-load and full-load operation before the voltage sag. The current instruction value under different operating conditions of voltage asymmetric sag can be calculated by (9), (10) and (15), as shown in Table 3.

3.2.1 PET no load before voltage sag

Figure 16 shows the waveform of the positive sequence current *dq*-axis component in the forward rotation coordinate system, which runs at no load before the voltage asymmetric sags. The current inner loop can quickly and accurately track the inner loop current instruction value within 5 ms, and can adjust the q-axis current to inject reactive power into the grid. The corresponding three-phase current waveform is shown in Fig. 17. Because of the negative sequence current elimination,

Fig. 19 Negative sequence *dq*-axis current when the voltage drops under full load condition
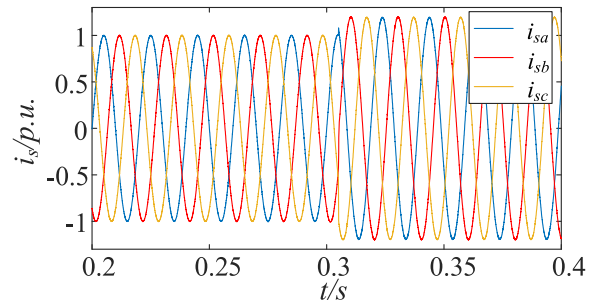
Fig. 20 Three-phase grid-connected current when the voltage drops under full load condition

the three-phase current can be injected symmetrically into the grid and reduce the impact on the grid.

#### 3.2.2 PET full load before voltage sag

As shown in Table 3, the PET in full load condition before the voltage asymmetry sag is simulated according to the power transmission direction. Figures 18 and 19 are waveforms of positive and negative sequence current dq axis components in the forward and reverse coordinate systems in the case where PET absorbs active power. It can be seen that the positive sequence current can quickly follow the instruction value change within 5 ms, and the negative sequence current inner loop can quickly eliminate the negative sequence current after the voltage sags.

Figure 20 and Fig. 21 are three-phase current waveforms and power waveforms in the case where PET injects active power into the AC system. It can be seen that the negative sequence flow elimination control strategy can ensure the symmetry of the current injected into the grid under the condition of asymmetric voltage sag. PET can perform reactive power compensation to the grid to assist the grid voltage recovery, maintain the active power level as far as possible to reduce the disturbance to the grid.

In the simulation model, the DC bus voltage is controlled by a 5 MW energy storage system connected to
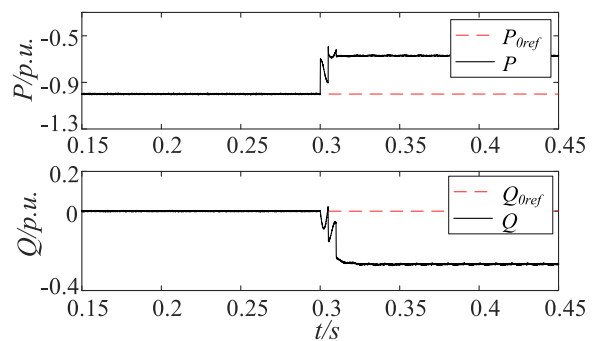
Fig. 21 Power waveform when the voltage drops under full load condition
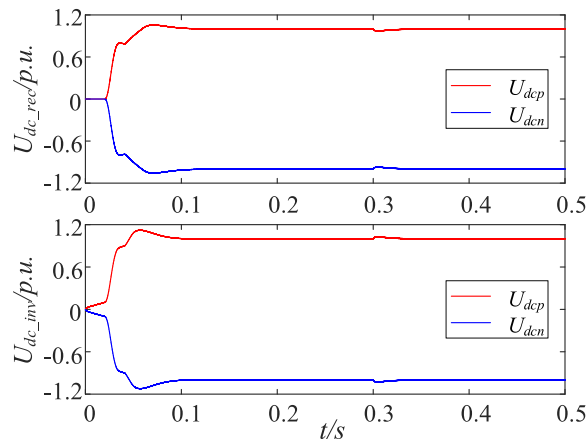
Fig. 22 DC bus voltage waveform during LVRT operation of PET

the same bus. The DC bus voltage waveform of the PET during LVRT operation under rectification and inverter conditions is given in the Fig. 22. It can be seen that under the joint action of the energy storage system and the PET, the DC bus voltage can be kept constant.

4 Conclusion

In this paper, a LVRT strategy that is suitable for power bidirectional transmission of PET is proposed, the effectiveness of which under voltage symmetric and asymmetric sag conditions is verified by simulation model. This strategy mainly implements the following functions:

1) During the voltage sag of the PET AC side, the power or voltage outer loop is blocked, and the current inner loop instruction value is given directly, which can improve the overall response speed of the system.
2) During the voltage asymmetric sag, the negative sequence current is eliminated to ensure the symmetry of the current injected into the grid.
3) According to the degree of positive sequence voltage sag, the corresponding reactive current injection is performed to help the grid voltage recover.
4) According to the active power condition before the voltage sag, the level and direction of active power are kept as far as possible within the upper limit of the current-carrying, and the disturbance to the AC and DC grids is reduced.

Abbreviations
LVRT: Low voltage ride through; MMC: Modular Multilevel Converter; PCC: Point of common connection; PET: Power electronic transformer; PLL: Phase-locked loop

Acknowledgements
Not applicable

Author's information
J. X. Han (1995-), male, he is currently working toward the Ph.D. degree at Huazhong University of Science and Technology. Major in the power system protection and control.
X. P. Kong (1988-), male, PHD and Engineer, Major in the DC control protection system and application of power electronic equipment in power grid.
P. Li (1982-), male, PHD and Engineer, Major in the UPFC control and protection system, DC control and protection system, power system protection and control.
Z. Zhang (1962-), male, PHD and Professor, Major in the protective relaying and electric and electronic technology.
X. G. Yin (1954-), male, PHD and Professor, Major in the protective relaying and power system stability control.

Author details
[1]State Key Laboratory of Advanced Electromagnetic Engineering and Technology, Huazhong University of Science and Technology, Wuhan 430074, Hubei, China. [2]State Grid Jiangsu Electric Power Co. Ltd., Research Institute, Nanjing 211103, Jiangsu, China.

References
1. Jiang, D., & Zheng, H. (2012). Research status and developing prospect of DC distribution network. *Automation of Electric Power Systems, 36*(8), 98–104.
2. Bruce, N., & Ken, C. (2016). DC local power distribution: Technology, deployment, and pathways to success. *IEEE Electrification Magazine, 4*(2), 29–36.
3. Li, Z., Gao, F., Zhao, C., et al. (2018). Research review of power electronic transformer technologies. *Proceedings of the CSEE, 38*(5), 1274–1289.
4. Xu, S., Alex, Q. H., & Rolando, B. (2013). Review of solid-state transformer technologies and their application in power distribution systems. *IEEE Journal of Emerging and Selected Topics in Power Electronics, 1*(3), 186–198.
5. Md, R. I., Youguang, G., & Jianguo, Z. (2014). A high-frequency link multilevel cascaded medium- voltage converter for direct grid integration of renewable energy systems. *IEEE Transactions on Power Electronics, 29*(8), 4167–4182.
6. Shi, J., Gou, W., Yuan, H., et al. (2011). Research on voltage and power balance control for cascaded modular solid-stated transformer. *IEEE Transactions on Power Electronics, 26*(4), 1154–1166.
7. Zhao, T., Wang, G., Bhattacharya, S., et al. (2013). Voltage and power balance control for a cascaded H-bridge converter-based solid-state transformer. *IEEE Transactions on Power Electronics, 28*(4), 1523–1532.
8. Sun, Y., Li, Y., Liu, J., et al. (2018). Coordinative control strategy for cascaded power electronic transformer. *Proceedings of the CSEE, 38*(5), 1290–1300.
9. Wang, D., Mao, C., & Lu, J. (2007). Auto-balancing electronic power transformer. *Proceedings of the CSEE, 27*(6), 77–83.

10. Jie, T., Chengxiong, M., Dan, W., et al. (2015). Analysis and control of electronic power transformer with star-configuration under unbalanced conditions. *IET Electric Power Applications, 9*(5), 358–369.

11. Feng, Y., Wu, J., Wang, X., et al. (2016). Control strategy of power electronic transformer under unbalanced grid fault. *Electric Power Construction, 37*(7), 84–90.

12. Hossein, D. T., Ali, I. M., Georgios, K., et al. (2016). Low-voltage ride-through capability of cascaded H-bridge multilevel converters for large-scale photovoltaic power plants. *IEEE Innovative Smart Grid Technologies-Asia (ISGT-Asia), 2016*, 52–57.

13. Li, Z., Wang, P., Chu, Z., et al. (2013). Research on medium- and high-voltage smart distribution grid oriented power electronic transformer. *Power System Technology, 37*(9), 2592–2601.

14. Jee-Hoon, J., Ho-Sung, K., Myung-Hyo, R., & Ju-Won, B. (2013). Design methodology of bidirectional CLLC resonant converter for high-frequency isolation of DC distribution systems. *IEEE Transactions on Power Electronics, 28*(4), 1741–1755.

15. Chen, Q., Ji, Y., & Wang, J. (2014). Analysis and Design of Bidirectional CLLLC resonant DC-DC transformers. *Proceedings of the CSEE, 34*(18), 2898–2905.

16. Kong, X., Zhang, Z., Yin, X., et al. (2013). Study on fault current characteristics and fault analysis method of power grid with inverter interfaced distributed generation. *Proceedings of the CSEE, 33*(34), 65–74.